ACS APPLIED MATERIALS & INTERFACES

www.acsami.org

Research Article

A Spin-Coated Hydrogel Platform Enables Accurate Investigation of Immobilized Individual Single-Walled Carbon Nanotubes

Matthew Card, Mitchell Gravely, S. Zahra M. Madani, and Daniel Roxbury*

Cite This: https://doi.org/10.1021/acsami.1c06562

Read Online

ACCESS | Metrics & More | Article Recommendations | Supporting Information

ABSTRACT: Single-walled carbon nanotubes (SWCNTs) have been used in a variety of sensing and imaging applications over the past few years due to their unique optical properties. In the solution phase, SWCNTs are employed as near-infrared (NIR) fluorescence-based sensors of target analytes via modulations in emission intensity and/or wavelength. In an effort to lower the limit of detection, research has been conducted into isolating SWCNTs adhered to surfaces for potential single molecule analyte detection. However, it is known that SWCNT fluorescence is adversely affected by the inherently rough surfaces that are conventionally used for their observation (e.g., glass coverslip), potentially interfering with fluorescence-based analyte detection. Here, using a spin-coating method with thin films of alginate and SWCNTs, we demonstrate that a novel hydrogel platform can be created to investigate immobilized individual SWCNTs without significantly perturbing their optical properties as compared to solution-phase values. In contrast to the glass coverslip, which red-shifted DNA-functionalized (6,5)-SWCNTs by an average of 3.4 nm, the hydrogel platform reported emission wavelengths that statistically matched the solution-phase values. Additionally, the heterogeneity in the wavelength measurements, as determined from the width of created histograms, was reduced nearly by a factor of 3 for the SWCNTs in the hydrogel platform when compared to glass coverslips. Using long SWCNTs, i.e., those with an average length above the diffraction limit of our microscope, we show that a glass coverslip can induce optical heterogeneity along the length of a single SWCNT regardless of its surface functionalization. This is again significantly mitigated when examining the long SWCNTs in the hydrogel platform. Finally, we show that upon the addition of a model analyte (calcium chloride), the optical response can be spatially resolved along the length of a single SWCNT, enabling localized analyte detection on the surface of a single nanoscale sensor.

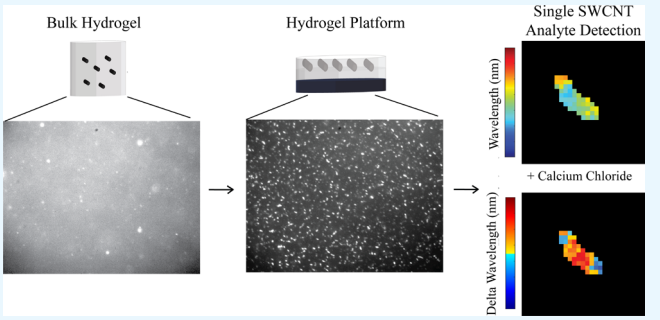

KEYWORDS: *single-molecule detection, optical sensors, hyperspectral imaging, near-infrared fluorescence, single-walled carbon nanotubes, hydrogel, spin coating*

INTRODUCTION

Semiconducting single-walled carbon nanotubes (SWCNTs) have emerged as tunable sensors for both *in vitro* and *in vivo* use due to their unique optical properties.[1−3] Their band-gap photoluminescence (fluorescence) is dependent on their (*n*,*m*) designated species (chirality) and has been touted for its inherent photostability and sensitivity to the SWCNT local environment, in addition to residing within the tissue-transparent near-infrared (NIR) region of the spectrum.[4] SWCNTs are inherently hydrophobic and will spontaneously aggregate in solution.[5] As such, a variety of strategies have been developed to disperse SWCNTs by functionalizing their hydrophobic surfaces. Noncovalent functionalization of SWCNTs with surfactants,[6] polymers,[7] nucleic acids,[8] or peptides[1] can effectively disperse them in aqueous solution and impart analyte selectivity without compromising their optical properties.[1] Exploiting these desirable properties, SWCNT-based sensors have recently been developed for various biosensing applications. Recently, Kruss et al. have developed an aptamer-wrapped SWCNT sensor to selectively detect serotonin release from cells.[9] A DNA-functionalized SWCNT (DNA-SWCNT) sensor conjugated with antibodies was fabricated by Heller et al. to detect the cancer biomarker urokinase plasminogen activator.[10] DNA-SWCNTs are especially prevalent in biosensing applications due to their enhanced biocompatibility,[11] ease of modification,[12] and superior stability.[13] In the solution phase, SWCNTs have been used to selectively detect analytes by measuring the variations in fluorescence properties caused by conformational

Received: April 9, 2021
Accepted: June 21, 2021

changes of the functionalization near the nanotube surface.[14] These measurements include, but are not limited to, integrated fluorescence intensity, emission wavelength, and full-width at half-maximum (FWHM). However, it is well known that SWCNT samples exhibit optical heterogeneity due to their varying physical parameters (i.e., chirality,[15] length,[16] and presence of defects[17]). Many recent studies have been conducted to create SWCNT samples of pure chirality or to sort them based on their length in order to improve their sensing capabilities.[18−20]

With all of the carbon atoms effectively residing on the surface, SWCNTs are especially sensitive to single molecules of analytes.[21] Single-molecule fluorescence-based analyte detection has been accomplished for hydrogen peroxide[2] and several neurotransmitters such as dopamine.[22] In these and other applications, it is desirable to maximize the capabilities of SWCNTs to lower the analyte limit of detection (LOD). To accomplish this, it is important to characterize individual SWCNTs to observe their intrinsic sensitivity and heterogeneity in response to an analyte. Previous studies have immobilized SWCNTs on glass coverslips to observe the changes in their fluorescence properties.[22−25] However, since SWCNTs are inherently sensitive to their local environment, interactions with the environment or glass surfaces can fundamentally change their optical properties (i.e., in the form of emission peak shifts and/or fluctuations in intensity) in the absence of a target analyte.[26−28] Smoother surfaces such as quartz and coatings on glass using specific protein interactions have been tested instead but are too expensive, specific (i.e., requiring a biotin protein on the SWCNT), or time-consuming for practical use.[29,30] Recent investigations of individual SWCNTs have shown that photoluminescence modulation occurs in a delocalized fashion along a single SWCNT.[31] Wang et al. have shown the use of wavelength maps for single SWCNTs and the increased sensitivity they have over intensity measurements due to heterogeneous changes in response to the dielectric environment.[32] Furthermore, the addition of certain solutions may remove the SWCNTs from the glass surface. Strong surfactants such as sodium deoxycholate (DOC) can exchange with DNA strands on SWCNTs bound to glass, subsequently forcing their removal from the surface.[33] The immobilization of SWCNTs on a solid support may therefore not be the best method to analyze individual SWCNT properties. There is thus an unmet need for a new method of immobilizing SWCNTs that can promote the acquisition of single SWCNT fluorescence properties in a perturbation-free manner.

Hydrogels are crosslinked networks of polymers suspended in water. They are intrinsically flexible and stable and present an aqueous phase that can be used to simulate solution-phase measurements.[34,35] Further, they are easily modifiable in terms of porosity, size, strength, and water content.[36] Due to these advantages, hydrogels can be used to simultaneously replicate an aqueous environment and immobilize SWCNTs without significantly altering their fundamental optical properties.[4,37] It has been reported previously that individual SWCNTs can be interrogated in a hydrogel; however, the method was extremely low-throughput.[37] To obtain proper optical characterization of individual SWCNTs, it is integral to retain them in one single plane of the hydrogel, limiting interference from out-of-focus SWCNTs. Spin coating, a process by which a solute is evenly distributed onto a surface using centripetal force that completely evaporates the solvent,[38] can accomplish this goal. In the case of hydrogels, the amount of water evaporated can be modified based on the application, ultimately creating a uniform, thin film of hydrogel.

Here, we report a four-step process to obtain a spin-coated hydrogel platform for accurate analysis of individual immobilized nanosensors. We show that while SWCNTs dispersed in a bulk hydrogel were not amenable for single-SWCNT analysis, the optimized spin-coated hydrogel platform contained DNA-SWCNT hybrids with minimal out-of-plane fluorescence. Analyzing the individual (6,5)-SWCNT spectra, DNA-SWCNT hybrids on glass coverslips displayed a significant red-shift in emission and a concomitant increase in spectral heterogeneity as compared to SWCNTs in the spin-coated hydrogel sample, which statistically matched solution-phase parameters. Upon addition of calcium chloride, DNA-SWCNT hybrids in our hydrogel platform more closely paralleled the solution-phase shift in emission wavelength when compared to SWCNTs on glass coverslips. We also analyzed long SWCNTs, i.e., those longer than the optical diffraction limit of our system, to show the inherent spectral heterogeneity along individual SWCNTs. Surfactant-wrapped SWCNTs, with a presumed micellar structure, showed a marked decrease in spectral heterogeneity in the hydrogel platform due to the relatively homogeneous surface morphology of the surfactant-SWCNT system.[16] Finally, upon interrogating a single long DNA-SWCNT hybrid before and after calcium addition, a wavelength map was created to show heterogeneous shifts due to different local calcium concentrations and variations in the surrounding environment. Thus, our spin-coated SWCNT-hydrogel platform can be used not only to investigate the nature of individual SWCNT properties but also as a highly sensitive detection device that mimics existing bulk and solution-phase data, potentially improving on current difficulties therein.

RESULTS AND DISCUSSION

To image individually dispersed and immobilized SWCNTs in an aqueous environment, we fabricated a spin-coated hydrogel platform (herein referred to as "hydrogel platform"). As described in the four-step process shown in Figure 1, a glass coverslip was first cleaned with ethanol and then treated with a dilute poly-L-lysine (PLL) solution. An alginate solution containing crosslinking agents was mixed with an initiator and quickly spin-coated onto the cleaned coverslip. After drying, a prepared DNA-SWCNT solution (see Materials and

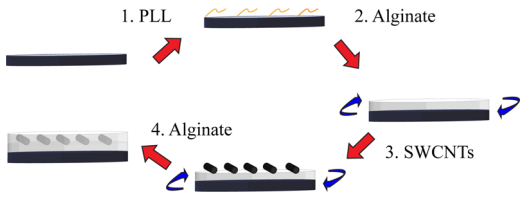

Figure 1. Schematic of the novel spin-coated SWCNT-hydrogel platform. (1) A glass coverslip was first cleaned with a 70% ethanol solution (EtOH) and subsequently immersed in poly-L-lysine (PLL) to promote adherence of the alginate solution. (2) The crosslinking of the alginate solution was initiated, and the resulting solution was shortly thereafter spin-coated onto the coverslip. The solution was left to dry to ensure consistency between samples. (3) A dilute solution of SWCNTs was then spin-coated onto the surface of the alginate. (4) Finally, a layer of alginate hydrogel was deposited on top to prevent the leakage of the SWCNTs.

https://doi.org/10.1021/acsami.1c06562
ACS Appl. Mater. Interfaces XXXX, XXX, XXX−XXX

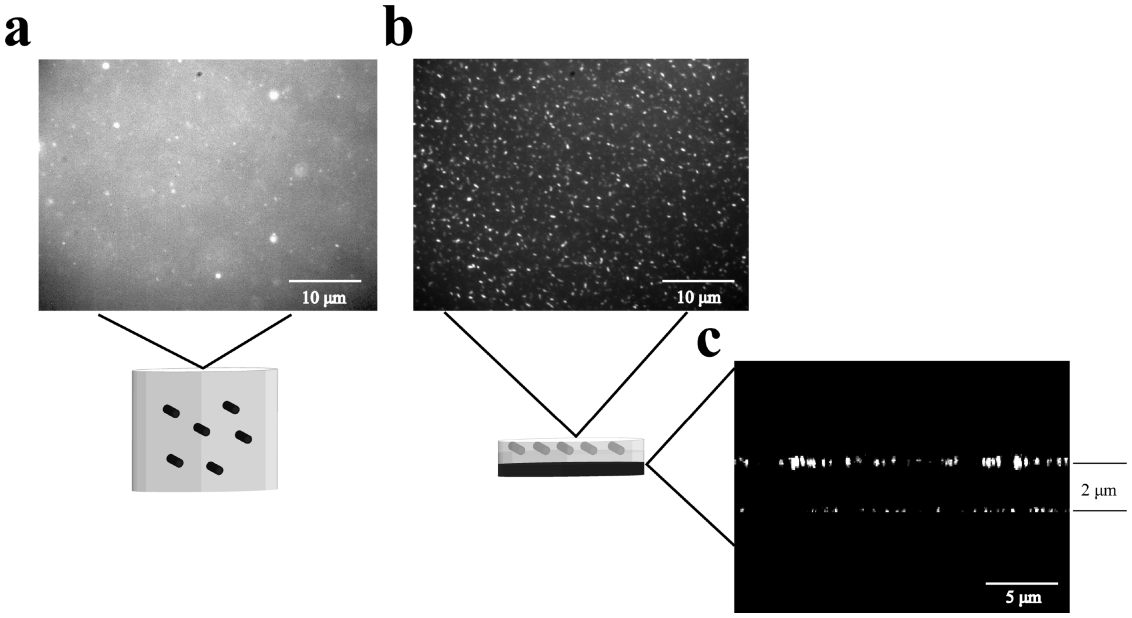

Figure 2. Broadband NIR fluorescence images of DNA-SWCNTs in different hydrogel systems. (a) Broadband image of SWCNTs mixed into a bulk hydrogel at 100× magnification demonstrating out-of-focus fluorescence. (b) Top-down and (c) side-on NIR fluorescence images of SWCNTs in the spin-coated hydrogel platform. A bottom layer of SWCNTs was deposited onto the glass coverslip to show the thickness of the spin-coated alginate hydrogel layer.

Methods) was subsequently spin-coated onto the alginate-coated glass, followed by a second layer of deposited alginate. The addition of the positively charged PLL was deemed critical to ensure proper adhesion between the alginate and the glass, both negatively charged.[39] Alginate was chosen for this study instead of other common hydrogels (e.g., agarose) due to its stronger covalent crosslinking, which is advantageous in spin-coated films.[35] The first alginate layer is left to dry to produce a homogeneous layer for the SWCNTs to interact with and limits diffusion to the glass surface. The second alginate layer rehydrates the bottom alginate layer, better representing solution-phase behavior, and also acts as a physical barrier to prevent removal of the SWCNTs upon addition of various solutions. All data were obtained from hydrogels in their "swelled" state with excess water to prevent evaporation due to the heat of the near-infrared laser (Figure S1).

We next performed near-infrared (NIR) fluorescence microscopy to characterize the hydrogel platform. When mixed into a bulk alginate hydrogel and imaged under 100× magnification, the majority of DNA-SWCNTs, as indicated by their broadband NIR fluorescence emission upon 730 nm laser excitation, were out of focus and thus gave rise to significant levels of background fluorescence, which made analysis of individual SWCNTs impossible (Figure 2a). In direct contrast, a broadband NIR fluorescence image of DNA-SWCNTs within the hydrogel platform (Figure 2b) demonstrated a reduction of out-of-focus fluorescence emission. By precisely controlling the *z*-position of the piezo stage on an inverted fluorescence microscope, a "*z*-stack" of NIR fluorescence images was created for the optimized hydrogel platform. A side-on representation of this *z*-stack is found in Figure 2c, in which an additional layer of SWCNTs was deposited onto the glass coverslip to gauge the thickness of the spin-coated alginate layer. Efforts were made to optimize the concentration of SWCNTs, spin-coater speed (RPM), alginate concentration, and crosslinking duration to obtain a single in-focus layer of well-dispersed SWCNTs (Figure S2). For example, increasing the spin-coater RPM for the SWCNT deposition step decreased the apparent density of SWCNTs in the hydrogel platform, thus decreasing the propensity for overlapped or aggregated SWCNTs. Too low of a local SWCNT density would additionally be undesirable due to reduced sampling. This side-on representation shows nearly no diffusion of SWCNTs above or below the spin-coated SWCNT layer.

To evaluate if certain subpopulations of SWCNTs preferentially adsorb to the hydrogel during the spin-coating process, we compared the fluorescence properties of SWCNTs cast in a bulk hydrogel to those in the spin-coated hydrogel. The center wavelength values of SWCNTs in the hydrogel platform and SWCNTs in the bulk hydrogel were found to be statistically identical (Figure S3). The same process was performed with DOC-functionalized SWCNTs, a second noncovalent SWCNT functionalization with a known homogeneous surface morphology.[40] The resultant center wavelength values were also nearly identical (Figure S4). We can therefore translate these findings to conclude that we do not observe any inherent bias due to surface chemistry when spin coating. We further compared the spatial orientation of SWCNTs by utilizing a polarizing filter and rotatable half-wave plate on the excitation laser (Figure S5). We found that while there was some alignment of the SWCNTs on glass coverslips, SWCNTs in the hydrogel platform showed little evidence of alignment. We anticipate that the less oriented nature of SWCNTs in the hydrogel platform is due to the lower spin-coat speeds used to obtain an optimal concentration of SWCNTs.

The potential for SWCNT diffusion through the alginate was further investigated by comparing the average size of our DNA-SWCNTs (~100 nm)[16] to the mesh size of the spin-coated hydrogel layer. The mesh size was found by using a swelling ratio correlation, similar to a previously described method.[41] The swelling ratio (q_F) was determined by:

$$q_F = \frac{m_{\text{wet}}}{m_{\text{dry}}} \tag{1}$$

https://doi.org/10.1021/acsami.1c06562
ACS Appl. Mater. Interfaces XXXX, XXX, XXX−XXX

where m_{wet} is the mass of the wet hydrogel, and m_{dry} is the mass of the dry hydrogel. The volume fraction of the polymer (v_2) can then be calculated by using:

$$v_2 = \frac{1}{1 + (q_F - 1)\rho_p/\rho_w} \quad (2)$$

where ρ_P and ρ_W are the densities of alginate (1.601 g/cm^3) and water (1 g/cm^3), respectively.

The crosslink density (n) was determined by:

$$n = -[\ln(1 - v_2) + v_2 + \chi_1 v_2^2]/[V_1(v_2^{1/3} - 0.5v_2)] \quad (3)$$

where χ_1 is the Flory–Huggins interaction parameter (0.5), and V_1 is the molar volume of water (18 cm^3). Finally, the mesh size (ξ) can then be approximated by using the following equation:

$$\xi = v_2^{-1/3} l \times \left[\left(\frac{2\rho_P}{n}\right)/M_r\right]^{1/2} C_n^{1/2} \quad (4)$$

where l is the carbon–carbon bond length of the alginate monomer (5.15 Å), M_r is the molecular weight of the repeat unit (390.1 g/mol), and C_n is the characteristic ratio (21.1) for alginate.[41] The swelling ratio was experimentally determined to be about 2 ± 0.1; thus, the mesh size was calculated to be 56 nm (Figure S6), lower than the average size of the examined DNA-SWCNTs. Therefore, we expect minimal diffusion of most single SWCNTs throughout our hydrogel platform.

To compare the utility of the optimized hydrogel platform to existing approaches, we contrasted the spectral data of DNA-SWNCTs in the platform to those deposited onto glass coverslips or in the solution phase. In addition to the fabrication of the hydrogel platform as described above, DNA-SWCNTs were deposited onto a glass coverslip and subsequently washed and dried. The samples were then imaged on an NIR fluorescence hyperspectral microscope under 730 nm laser excitation to acquire "hyperspectral cubes" of emission data in the wavelength range of 950–1050 nm.[42] Regions of interest (ROIs) were selected that best exhibited spatially distinct single SWCNTs (Figure S7). The average spectrum of each ROI was extracted and fitted using a Lorentzian line shape, and the emission center wavelengths were compiled into histograms (Figure 3). The extracted data for each ROI additionally included FWHM and maximum intensity, and several graphs were constructed to investigate potential correlations (Figures S8 and S9). There was determined to be a small positive correlation between wavelength and FWHM. The spectra that showed multiple peaks were determined to be aggregates of SWCNTs and were subsequently removed from the results. The average center wavelength for DNA-SWCNTs on glass (997.7 ± 4.67 nm; mean ± s.d. of n = 300 ROIs) showed a red-shift (shift to longer wavelength) of 3.4 nm when compared to that of DNA-SWCNTs in solution (994.3 ± 0.5 nm; mean ± s.d. of n = 3 spectra) (Figure 3a). The center emission wavelength for our hydrogel platform (995.3 ± 1.7 nm) displayed a small red-shift when compared to the solution-phase value, but this difference was not statistically significant (Figure 3b). We further fitted a Gaussian curve to each wavelength histogram to compare the heterogeneity (width, "σ") of values in each condition. The σ-value of DNA-SWCNTs deposited onto glass showed a 3-fold increase when compared to the hydrogel platform. We attribute the red-shift of DNA-SWCNTs on glass coverslips

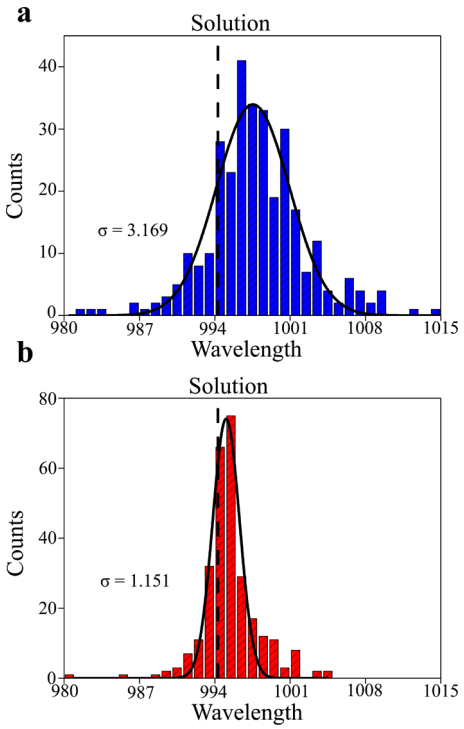

Figure 3. Fitted optical properties of populations of single (6,5) DNA-SWCNTs. Histograms of fitted emission center wavelengths of SWCNTs (a) deposited onto glass coverslips or (b) embedded in the hydrogel platform. The dotted black lines represent the center wavelength of the DNA-SWCNTs in solution (λ = 994.3 ± 0.5; mean ± s.d.). The solid black lines represent Gaussian fits with widths (σ) denoted on the graphs.

to the direct contact with the hard charged surface of glass, which modulates the local dielectric environment and inhibits conformational changes of the DNA strand.[43] Furthermore, the increased σ-value of DNA-SWCNTs on glass coverslips demonstrates the increased heterogeneity in the local environment of the DNA-SWCNTs when bound to the rough glass surface (Figure S10). While alginate is additionally composed of charged carboxylate groups and crosslinking agents, we propose that the aqueous-like phase of the hydrogel prevents close contact of the charged groups. A large portion of the active charge would be present on uncrosslinked polymer ends near the surface,[44] leading to the observed close agreement in DNA-SWCNT emission wavelengths between the hydrogel platform and solution values (Figure S11).

Due to their ability to electrostatically crosslink DNA on the surface of SWCNTs and cause a wavelength and/or intensity change,[45] calcium ions were used as a model analyte to demonstrate the sensing capacities of our hydrogel platform. We used higher concentrations than those that have been used in recent applications[45,46] to more clearly demonstrate the proposed limitations of DNA-SWCNTs on a glass surface. A high concentration of calcium chloride (1 M) was aliquoted onto the concave hydrogel platform where a small slit was added to prevent any runoff of the solution. ROIs of presumably single SWCNTs were selected as previously mentioned, and the spectra for each were extracted both before and after addition of calcium chloride (Figure 4a,b). Notably, the spatial positions of the ROIs remained fixed after addition of the analyte, owing to the stability of the SWCNTs in the hydrogel platform. Figure 4c–e shows the fitted spectra

https://doi.org/10.1021/acsami.1c06562
ACS Appl. Mater. Interfaces XXXX, XXX, XXX–XXX

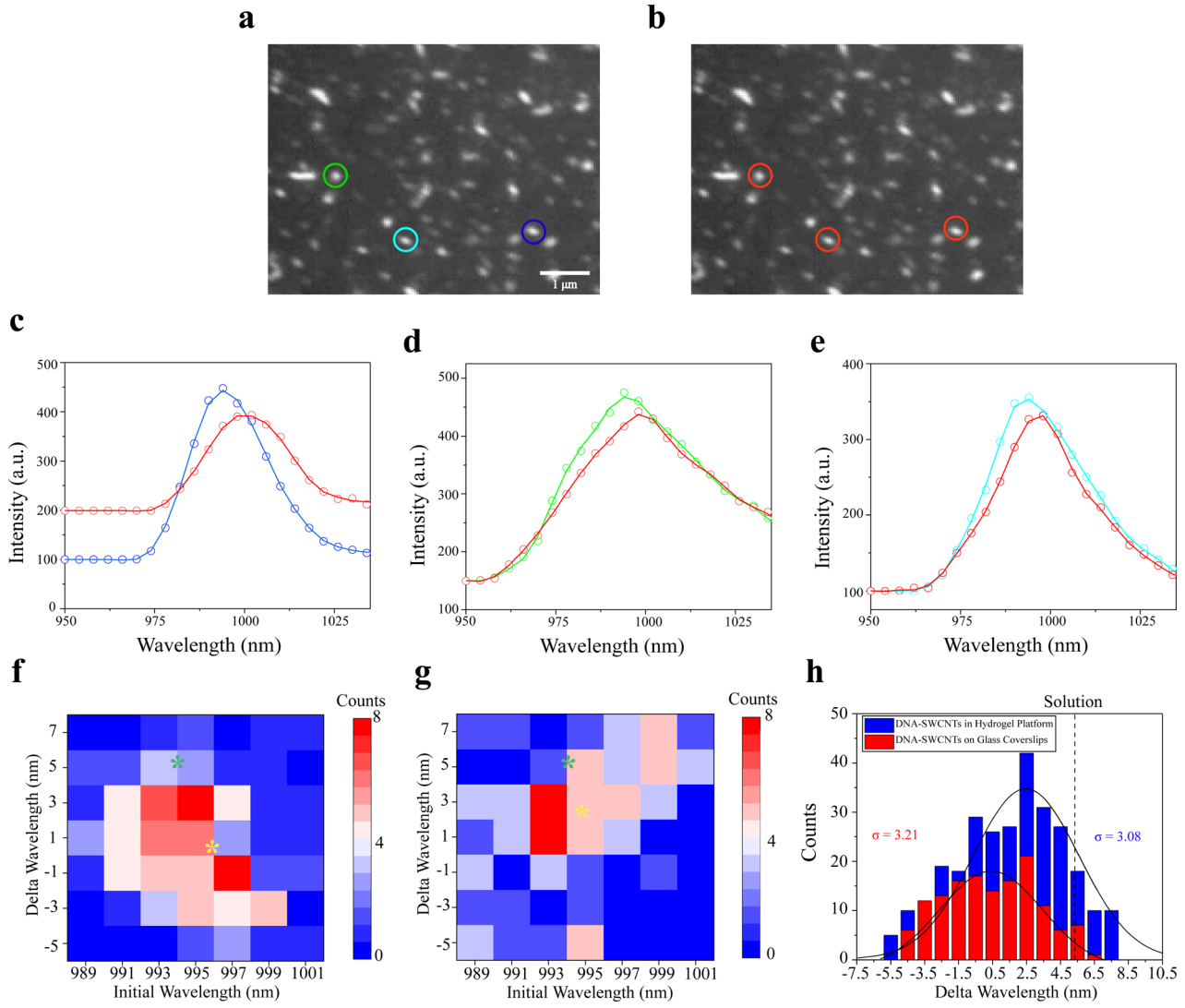

Figure 4. Single DNA-SWCNT calcium detection. Magnified broadband NIR fluorescence images of individual SWCNTs in the hydrogel platform (a) before and (b) after addition of 1 M calcium chloride. The green, blue, and cyan circles each designate a single region of interest (ROI), presumably a single SWCNT, that is again found in the image after calcium addition (red circles). (c−e) Fluorescence spectra of chosen ROIs before and after calcium addition. Delta wavelength (nm) vs initial wavelength for individual SWCNTs (f) on glass coverslips or (g) in the hydrogel platform after addition of calcium. The green and yellow asterisks denote the locations of the average solution-phase values and average hydrogel platform or glass values, respectively. (h) Stacked histogram of DNA-SWCNT delta wavelength on glass coverslips (red) or in the hydrogel platform (blue). The dotted line represents solution-phase data after addition of 1 M calcium chloride. The solid black lines represent Gaussian fits with widths (σ) denoted on the graphs.

for three chosen ROIs before and after the addition of calcium chloride.

To quantify the differences in sensor response between the glass coverslip and hydrogel platform systems, heatmaps (i.e., two-dimensional histograms) of the change in center wavelength upon addition of calcium (delta wavelength) versus initial center wavelength were constructed. DNA-SWCNTs on glass coverslips and in the hydrogel exhibited red-shifts of 0.38 ± 2.6 and 2.4 ± 3.1 nm, respectively (Figure 4f,g), while individual data points exhibited shifts as high as 5 or 7 nm, respectively. By creating a stacked histogram of the delta wavelength of SWCNTs on glass and in the hydrogel after calcium chloride addition (Figure 4h), the heterogeneity of each sample was quantified by fitting the data to Gaussian curves and obtaining σ-values. The σ-value for DNA-SWCNTs on glass was 3.21, while it was 3.08 for DNA-SWCNTs in the hydrogel platform. To confirm these findings with a second SWCNT preparation, the above analysis was repeated using (8,6) DNA-dispersed HiPco SWCNTs. Similar trends were observed in initial and calcium-modified center wavelength values of SWCNTs in the hydrogel platform and on glass coverslips (Figures S12 and S13). As a reference, various concentrations of calcium chloride were added to a solution of 1 mg/L DNA-SWCNTs, and 1 M calcium chloride was shown to cause a large wavelength red-shift of 5.3 ± 0.3 nm (Figure S14). In contrast to the concentration-dependent red-shifting, changes in solution-phase fluorescence intensity did not follow a definite trend at higher calcium chloride concentrations. This could be explained by the dynamic interactions that occur in the solution environment, leading to both the localized formation of aggregates and regions of decreased SWCNT concentrations, ultimately producing highly variable fluorescence intensities within a single solution (Figure S15). The small average emission wavelength shift of DNA-SWCNTs on

https://doi.org/10.1021/acsami.1c06562
ACS Appl. Mater. Interfaces XXXX, XXX, XXX−XXX

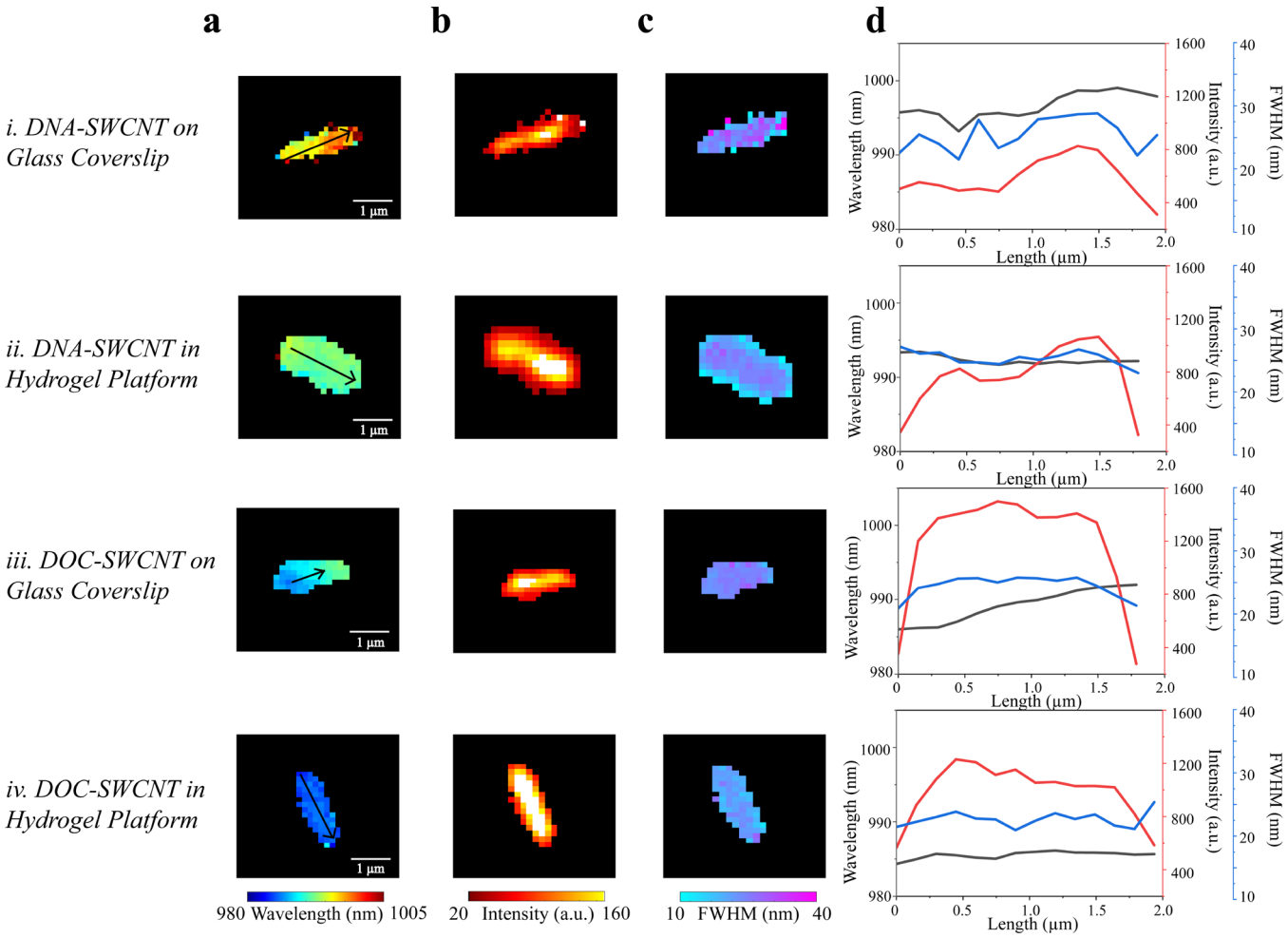

Figure 5. Optical properties along individual long SWCNTs. (a) Wavelength, (b) intensity, and (c) FWHM maps of DNA- or DOC-dispersed SWCNTs deposited onto glass or embedded in the SWCNT-hydrogel platform. (d) Line profiles of each respective map for a given SWCNT.

glass can be attributed to the inhibition of DNA strand reorganization due to physical and electrostatic interactions with the charged glass surface. The average wavelength shift of DNA-SWCNTs in the hydrogel platform gave a somewhat muted response compared to that of DNA-SWCNTs in the solution phase. We propose that due to the immobilization of DNA-SWCNTs in the hydrogel, analyte-induced aggregation (Movie S1) is significantly reduced or removed completely, preventing previously observed resultant red-shifts.[47] We hypothesize that the delta wavelength distribution of DNA-SWCNTs on glass is only slightly broader due to the aforementioned inability of calcium ions to modulate DNA on the SWCNT surface. DNA-SWCNTs in our hydrogel platform thus have an increased sensitivity compared to those on glass coverslips. Moreover, the further limiting of solution-phase aggregation effects makes our platform aptly suited for a variety of sensing applications.

We next employed the optimized hydrogel platform to investigate spectral features along the length of single SWCNTs. Aqueous dispersions of SWCNTs were fabricated by short periods of sonication (5 min) with either DNA or DOC. The shorter sonication time reduced the propensity for sonication-induced scission of the SWCNTs, ensuring the observation of SWCNTs longer than the optical diffraction limit of our system (~500 nm). The herein referred to as "long SWCNT" samples were either incorporated into the hydrogel platform or deposited onto glass coverslips. Hyperspectral cubes were acquired and the spectra from each pixel of the SWCNTs were independently fitted to a Lorentzian line shape using custom MATLAB codes. The processed data were used to construct maps of emission center wavelength, intensity, and FWHM (Figure 5a–c). We note that the pixel size of our NIR detector is 150 nm, below the ~500 nm optical diffraction limit of SWCNTs emitting fluorescence near 1000 nm.[48] The resultant spectral data are inherently blurred across a minimum of 3 pixels. A line was manually drawn along the length of each SWCNT and the resultant line profiles were created for each spectral feature (Figure 5d). A striping pattern was observed within the wavelength map of the DNA-SWCNT on a glass coverslip, which was consistent in other examined samples of the same kind (Figure 5a(i) and Figure S16). The variations in emission center wavelength often propagated along the length of an SWCNT, reaching a minimum at one end and a maximum at the other. In contrast to the glass coverslip, the center wavelength profile along DNA-SWCNTs in the hydrogel platform (Figure 5a(ii) and Figure S17) showed a marked decrease in heterogeneity. The emission center wavelength map of DOC-SWCNTs on glass (Figure 5a(iii) and Figure S18) showed a similar striping pattern along the SWCNT, while DOC-SWCNTs in alginate (Figure 5a(iv) and Figure S19) demonstrated a very homogeneous pattern, with a maximum variation in wavelength along the length of a single

https://doi.org/10.1021/acsami.1c06562
ACS Appl. Mater. Interfaces XXXX, XXX, XXX−XXX

SWCNT of no more than 1.5 nm. We believe that these findings illustrate the heterogeneous dielectric environment that the DNA-SWCNT experiences when pinned to the intrinsically rough glass coverslip surface. In contrast to the glass coverslip, the center wavelength values along DNA-SWCNTs in the hydrogel platform showed reduced heterogeneity, presumably due to the removal of hard contacts with the glass. DOC-SWCNTs on glass coverslips further support the idea that glass binding interactions cause heterogeneity on the surface of a SWCNT. The exact interactions between the glass surface and DOC are not well known, but we presume that the micellar structure present in solution is disrupted. The homogeneous nature of DOC-SWCNT surface morphology in the hydrogel platform is observed from the absence of major fluctuations in the corresponding wavelength profile.

In conjunction with the emission center wavelength maps and profiles, intensity and FWHM data were similarly obtained and analyzed. The intensity profiles of SWCNTs were generally parabolic, reaching a maximum near the center of the SWCNT (Figure 5b and Figures S16−S19). Intensity profiles that did not conform to this trend could be the result of certain defects on the SWCNT surface. The profiles of FWHM were seemingly random, and their profiles were very inconsistent (Figure 5c and Figures S9−S12). Based on these findings, it was difficult to draw further conclusions between center emission wavelength, intensity, and FWHM along a single SWCNT.

We next directly compared the heterogeneity in emission center wavelength along the length of long DNA- or DOC-SWCNTs either on glass coverslips or in the hydrogel platform. A delta wavelength value for each SWCNT was calculated by subtracting the lowest fitted center wavelength value from the highest center wavelength value. Across all conditions, individual SWCNTs of similar lengths (~2 um) were chosen for analysis. Figure 6 shows the distinct differences between the various conditions. DOC-SWCNTs in the hydrogel platform showed a remarkably small delta wavelength value of 1.5 ± 0.6 nm, which was significantly less ($p < 0.001$) than DOC-SWCNTs on glass coverslips, with a value of 5.0 ± 1.4 nm. DNA-SWCNTs showed a very similar trend, where the delta wavelength value was 6.1 ± 2.8 nm on glass coverslips, significantly more ($p < 0.01$) than the value of 2.3 ± 0.8 obtained from the hydrogel platform. Intensity and FWHM differences were also compiled and are shown in Figure S20. It is important to note that the wavelength difference for each condition is representative of the extent of heterogeneity present in the corresponding profile or map. This conforms to the idea that the glass surface generates greater spectral heterogeneity along and among single SWCNTs.

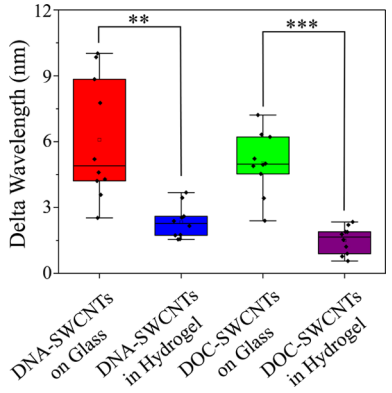

Figure 6. Change in wavelength (delta wavelength, nm) along the length of individual long SWCNTs. Each box contains 25−75% of data, the middle line represents the median, the open square represents the mean, and whiskers represent outliers. A two sample *t*-test at 95% confidence was performed to demonstrate significance. (***) significance is denoted by $p < 0.001$, and (**) significance is denoted by $p < 0.01$.

Finally, we demonstrate the spectral behavior along a single SWCNT in response to a model analyte that was added to the system. Emission center wavelength maps of an individual long DNA-SWCNT in the hydrogel platform were constructed before and after 1 M calcium chloride was spiked into the sample (Figure 7a,b). To account for slight shifts in spatial orientation of the SWCNT, the wavelength maps were aligned (translational and rotational) using a custom MATLAB code to maximize overlap (Figure S21). The fitted emission center wavelength of each pixel before calcium addition was subtracted from each corresponding pixel after calcium addition. The resulting wavelength map shows the delta wavelength values along a single SWCNT in response to analyte addition (Figure 7c). Interestingly, the initial average center emission wavelength of the SWCNT was 994.9 nm, and the average center emission wavelength after calcium addition was 995.9 nm. Despite this small average difference of 1 nm, the local wavelength differences are much larger across the length of the SWCNT. This shows the potential to lower the limit of detection for certain analytes by detecting localized optical modulations on portions of SWCNTs that would otherwise go unnoticed at the overall SWCNT level.

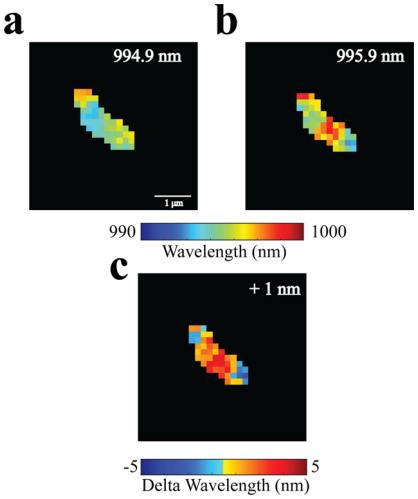

Figure 7. Single long DNA-SWCNT within the hydrogel platform in response to the addition of calcium chloride. Wavelength map of a long DNA-SWCNT (a) before calcium addition and (b) after calcium addition. (c) Wavelength map of the delta wavelength (after addition minus before addition) for each pixel. Overlap was maximized in MATLAB using a custom code. The value at the top right of each figure indicates the average.

CONCLUSIONS

In this study, we have demonstrated a novel method to obtain a single layer of SWCNTs without altering their fundamental optical properties. DNA-SWCNTs encapsulated in our hydrogel platform recapitulated the spectral data characteristic of the

https://doi.org/10.1021/acsami.1c06562
ACS Appl. Mater. Interfaces XXXX, XXX, XXX−XXX

solution phase, in stark contrast to the significant red-shift displayed by DNA-SWCNTs deposited onto a glass coverslip. This phenomenon is dependent on the stronger electrostatic interactions between SWCNTs on glass compared to SWCNTs in an alginate hydrogel. To investigate potential single-molecule detection applications, line profiles were created along sufficiently long SWCNTs to obtain an array of spectral data from single SWCNTs under the same conditions. DNA-SWCNTs in the hydrogel platform showed a reduction of heterogeneity in the optical properties, presumably as a result of removing several deleterious interactions between the hybrids and the glass surface. DOC-dispersed SWCNTs in the hydrogel platform more accurately demonstrated the optical homogeneity of the DOC functionalization, hinting at the use of this technology for SWCNT surface morphology applications. Lastly, calcium chloride was added to DNA-SWCNTs to demonstrate the potential for the sensing of relevant analytes. The inconsistency of analyte-dependent fluorescence changes on glass coverslips was extremely apparent. In contrast, our hydrogel platform gave results more consistent with the solution phase, with the notable exception of aggregation-induced effects, allowing for a more sensitive sensing platform. The small red-shift of the DNA-SWCNTs in the hydrogel platform after calcium addition when compared to solution exemplifies the potential to remove aggregation effects and other environmental factors that can lead to spectral heterogeneity in a given sample. Changes in emission wavelength in response to an analyte can be tracked along the length of a single SWCNT, lowering the apparent limit of detection by effectively increasing the resolution. Our hydrogel platform can thus be used to improve the sensing capabilities of conventional single SWCNT and solution-phase approaches. Limiting interference from the immobilizing substrate is critical to identify mechanisms of specific analyte-SWCNT interactions. Furthermore, we envision that this platform could enable more sensitive and selective detection of biologically relevant analytes, including bulky or complex biomolecules that interact with large nanotube areas.

MATERIALS AND METHODS

SWCNT Sample Preparation. Single-walled carbon nanotubes produced using the CoMoCAT or HiPco process were used throughout this study. For each dispersion, 1 mg of raw nanotubes was added to 2 mg of ss$(GT)_{15}$ oligonucleotide (Integrated DNA Technologies) and 1 mL of 100 mM NaCl (Sigma-Aldrich) or 10 mg of sodium deoxycholate (DOC, Sigma-Aldrich) with 1 mL of deionized water (DI) water in a microcentrifuge tube. The suspension was ultrasonicated with a 1/8 in. tapered microtip at 40% amplitude for 30 min (Sonics Vibracell VCX-130; Sonics and Materials) in a 0 °C temperature-controlled microcentrifuge holder. The dispersion was then ultracentrifuged (Sorvall Discovery M120 SE) for 30 min at 250,000*g*, and the top 80% of the supernatant was extracted. The concentration of each dispersion was determined using a UV/vis/NIR spectrophotometer (Jasco, Tokyo, Japan) and the extinction coefficient A910 = 0.02554 L mg^{-1} cm^{-1}.[13,14,16]

Hydrogel Platform Procedure. First, a 25 mm round glass coverslip was soaked with 70% ethanol for 5 min in a small Petri dish and rinsed with DI water. The coverslip was then soaked in a 250 μg/mL poly-L-lysine (PLL, Sigma-Aldrich) solution for 10 min and rinsed with DI. One milliliter of a 1.5% alginate (Sigma-Aldrich)/adipic acid dihydrazide (AAD, Sigma-Aldrich)/1-hydroxybenzotriazole (HOBt, Sigma-Aldrich) mixture was mixed with 0.5 mL of 100 mg/mL 1-ethyl-3-(3-dimethylaminopropyl)carbodiimide (EDC, Sigma-Aldrich) for 3 min to initiate crosslinking. AAD (8.8 mg) and HOBt (11.62 mg) were used per 200 mg of alginate. Alginate was purified and lyophilized prior to use, and 0.1 M 2-(*N*-morpholino)ethane sulfonic acid (MES, Sigma-Aldrich) was used as the solvent. The coverslip was taped onto a Petri dish cover and placed onto the spin-coater rotor (Laurell Model WS-400BZ-6NPP/LITE). The resulting solution was then deposited onto the coverslip at 2400 rpm for 30 s. The alginate was left to dry for 10 min. Two hundred microliters of 2 mg/L DNA-SWCNTs was subsequently spin-coated onto the dried alginate surface at 1400 rpm. A final 1 mL layer of 1% alginate/AAD/HOBt solution was mixed with EDC and deposited onto the bottom alginate surface. After adding 60 μL of DI water and 60 μL of a 2 mg/mL 6-hydroxy-2,5,7,8-tetramethylchroman-2-carboxylic acid (Trolox) solution, the hydrogel platform was used for further investigation of SWCNTs. To create the bulk hydrogel control found in Figure 2a, DNA-SWCNTs were mixed into alginate at a concentration of 5 mg/L and drop-casted onto a glass coverslip. The fabricated spin-coated hydrogel layers were also soaked in water for 24 h and used for swelling measurements.

SWCNT Glass Deposition. Sixty microliters of a 0.1 mg/L DNA or DOC-SWCNT solution was deposited on a 20 mm square glass coverslip for 30 s. The solution was removed and then rinsed with DI water. Sixty microliters of a 2 mg/mL Trolox solution was deposited onto the coverslip, and the sample was taken to the hyperspectral microscope for imaging.

Near-Infrared Fluorescence Microscopy. A near-infrared hyperspectral fluorescence microscope, similar to a previously described system,[14] was used to obtain hyperspectral data from individual SWCNTs. Briefly, a 730 nm diode laser with an output power of 1.5 W was reflected onto the stage of an Olympus 1X-73 inverted microscope using a UApo N 100×/1.49 oil immersion objective (Olympus, USA). The emission then passed through a volume Bragg Grating where it was collected by a 2D InGaAs array detector (Photon etc.), generating stacks of spectral images. For population data of short SWCNTs, samples of DNA-SWCNTs in the hydrogel platform or on glass coverslips were prepared as described above. A sample was mounted on the hyperspectral microscope and stacks of spectral images were acquired (wavelength range: 950−1050 nm; stepping size: 4 nm; exposure time: 2 s). For HiPco SWCNT data, the parameters used were as follows: wavelength range: 900−1350 nm; stepping size: 4 nm; exposure time: 1.5 s. For long SWCNT experiments, samples on glass were prepared by using a solution of 0.3 mg/L DNA-SWCNTs or DOC-SWCNTs and left for 20 min before washing with DI. Long SWCNTs in the alginate hydrogel were prepared using two spin-coating steps of 0.3 mg/L DNA-SWCNTs or DOC-SWCNTs following the first alginate layer. For polarized excitation studies, a linear polarizer (650−1100 nm) and achromatic half-wave plate (350−850 nm) were placed in the excitation path of the 730 nm laser. The half-wave plate was mounted on a precision rotation mount and rotated in steps of 15° from 0° to 180° with regard to the linear polarizer.

Atomic Force Microscopy. AFM images were acquired similar to a previous study.[16] Freshly cleaved mica was treated with amino-propyltriethoxysilane (AP) to produce AP-mica through the vapor deposition method. A 100 kDa Amicon centrifuge filter (Millipore) was used to remove free DNA from a solution of DNA-SCNTs. The resulting solution at a concentration of 2 mg/L was deposited on AP-mica for 4 min before it was rinsed with 10 mL of DI water. The AP-mica-deposited DNA-SWCNTs were then blown dry with argon gas. An AsylumMFP-3D-BIO AFM with an Olympus AC240TS probe was used for imaging in AC mode, and the data were captured with 2.93 nm/pixel *xy* resolution and 15.63 pm *z* resolution. Images were acquired at Memorial Sloan Kettering Cancer Center (MSKCC).

SWCNT Adsorption. To test for preferential adsorption of SWCNTs, a 5 mg/L DNA- or DOC-SWCNT bulk hydrogel was prepared as previously described and imaged with a 20× objective. This was compared to a population of single DNA- or DOC-SWCNTs in the spin-coated hydrogel platform.

Statistical Analysis. Statistical measurements and analyses were performed in OriginPro 2019 using two-sample *t*-tests under the null hypothesis. Lorentzian and Gaussian fits were also created using

https://doi.org/10.1021/acsami.1c06562
ACS Appl. Mater. Interfaces XXXX, XXX, XXX−XXX

OriginPro. Custom MATLAB codes were used for preparation of images and maps. ImageJ software was used for image analysis.

■ ASSOCIATED CONTENT

Supporting Information

The Supporting Information is available free of charge at https://pubs.acs.org/doi/10.1021/acsami.1c06562.

Figure S1: long-term stability of NIR fluorescence in the hydrogel platform; Figure S2: optimization of spin-coating parameters; Figure S3: DNA-SWCNTs in a bulk or spin-coated hydrogel; Figure S4: DOC-SWCNTs in a bulk or spin-coated hydrogel; Figure S5: orientation of DNA-SWCNTs; Figure S6: calculation of mesh size for spin-coated alginate hydrogels; Figure S7: sample ROI spectra and fitting; Figure S8: population data comparisons for DNA-SWCNTs; Figure S9: population data comparisons for DOC-SWCNTs; Figure S10: AFM image of a glass coverslip surface; Figure S11: demonstration of crosslinking between alginate layers; Figure S12: fitted optical properties of (8,6) DNA-SWCNTs. Figure S13: calcium detection with single (8,6) DNA-SWCNTs; Figure S14: solution-phase calcium response of DNA-SWCNTs; Figure S15: variations in the intensity of aggregated DNA-SWCNTs; Figure S16: additional line profiles for DNA-SWCNTs on glass; Figure S17: additional line profiles for DNA-SWCNTs in alginate; Figure S18: additional line profiles for DOC-SWCNTs on glass. Figure S19: additional line profiles for DOC-SWCNTs in alginate; Figure S20: variations in intensity and FWHM along single SWCNTs; Figure S21: pixel matrices of center wavelength along a single SWCNT (PDF)

Video of analyte-induced aggregation (AVI)

■ AUTHOR INFORMATION

Corresponding Author

Daniel Roxbury − *Department of Chemical Engineering, University of Rhode Island, Kingston, Rhode Island 02881, United States;* orcid.org/0000-0003-2812-3523; Email: roxbury@uri.edu

Authors

Matthew Card − *Department of Chemical Engineering, University of Rhode Island, Kingston, Rhode Island 02881, United States;* orcid.org/0000-0002-0471-0961

Mitchell Gravely − *Department of Chemical Engineering, University of Rhode Island, Kingston, Rhode Island 02881, United States;* orcid.org/0000-0001-7938-6054

S. Zahra M. Madani − *Department of Chemical Engineering, University of Rhode Island, Kingston, Rhode Island 02881, United States;* orcid.org/0000-0001-5435-4697

Complete contact information is available at: https://pubs.acs.org/10.1021/acsami.1c06562

Notes

The authors declare no competing financial interest.

■ ACKNOWLEDGMENTS

This work was supported by the National Science Foundation (CAREER Award #1844536 and EPSCoR Cooperative Agreement #OIA-1655221) and the University of Rhode Island College of Engineering.

■ REFERENCES

(1) Antonucci, A.; Kupis-Rozmyslowicz, J.; Boghossian, A. A. Noncovalent Protein and Peptide Functionalization of Single-Walled Carbon Nanotubes for Biodelivery and Optical Sensing Applications. *ACS Appl. Mater. Interfaces* **2017**, *9*, 11321−11331.

(2) Heller, D. A.; Jin, H.; Martinez, B. M.; Patel, D.; Miller, B. M.; Yeung, T. K.; Jena, P. V.; Höbartner, C.; Ha, T.; Silverman, S. K.; Strano, M. S. Multimodal Optical Sensing and Analyte Specificity Using Single-Walled Carbon Nanotubes. *Nat. Nanotechnol.* **2009**, *4*, 114−120.

(3) Pan, J.; Li, F.; Choi, J. H. Single-Walled Carbon Nanotubes as Optical probes for Bio-Sensing and Imaging. *J. Mater. Chem. B* **2017**, *5*, 6511−6522.

(4) Galassi, T. V.; Jena, P. V.; Roxbury, D.; Heller, D. A. Single Nanotube Spectral Imaging To Determine Molar Concentrations of Isolated Carbon Nanotube Species. *Anal. Chem.* **2017**, *89*, 1073−1077.

(5) Koh, B.; Cheng, W. Mechanisms of Carbon Nanotube Aggregation and the Reversion of Carbon Nanotube Aggregates in Aqueous Medium. *Langmuir* **2014**, *30*, 10899−10909.

(6) Vaisman, L.; Wagner, H. D.; Marom, G. The Role of Surfactants in Dispersion of Carbon Nanotubes. *Adv. Colloid Interface Sci.* **2006**, *128*, 37−46.

(7) Fong, D.; Adronov, A. Recent Developments in the Selective Dispersion of Single-Walled Carbon Nanotubes Using Conjugated Polymers. *Chem. Sci.* **2017**, *8*, 7292−7305.

(8) Zheng, M.; Jagota, A.; Semke, E. D.; Diner, B. A.; McLean, R. S.; Lustig, S. R.; Richardson, R. E.; Tassi, N. G. DNA-Assisted Dispersion and Separation of Carbon Nanotubes. *Nat. Mater.* **2003**, *2*, 338−342.

(9) Dinarvand, M.; Neubert, E.; Meyer, D.; Selvaggio, G.; Mann, F. A.; Erpenbeck, L.; Kruss, S. Near-Infrared Imaging of Serotonin Release from Cells with Fluorescent Nanosensors. *Nano Lett.* **2019**, *19*, 6604−6611.

(10) Williams, R. M.; Lee, C.; Heller, D. A. A Fluorescent Carbon Nanotube Sensor Detects the Metastatic Prostate Cancer Biomarker uPA. *ACS Sens.* **2018**, *3*, 1838−1845.

(11) Farrera, C.; Torres Andón, F.; Feliu, N. Carbon Nanotubes as Optical Sensors in Biomedicine. *ACS Nano* **2017**, *11*, 10637−10643.

(12) Sellner, S.; Kocabey, S.; Nekolla, K.; Krombach, F.; Liedl, T.; Rehberg, M. DNA Nanotubes as Intracellular Delivery Vehicles in Vivo. *Biomaterials* **2015**, *53*, 453−463.

(13) Safaee, M. M.; Gravely, M.; Lamothe, A.; McSweeney, M.; Roxbury, D. Enhancing the Thermal Stability of Carbon Nanomaterials with DnA. *Sci. Rep.* **2019**, *9*, 1−11.

(14) Gravely, M.; Safaee, M. M.; Roxbury, D. Biomolecular Functionalization of a Nanomaterial To Control Stability and Retention within Live Cells. *Nano Lett.* **2019**, *19*, 6203−6212.

(15) Liu, B.; Wu, F.; Gui, H.; Zheng, M.; Zhou, C. Chirality-Controlled Synthesis and Applications of Single-Wall Carbon Nanotubes. *ACS Nano* **2017**, *11*, 31−53.

(16) Safaee, M. M.; Gravely, M.; Rocchio, C.; Simmeth, M.; Roxbury, D. DNA Sequence Mediates Apparent Length Distribution in Single-Walled Carbon Nanotubes. *ACS Appl. Mater. Interfaces* **2019**, *11*, 2225−2233.

(17) Wang, Q. H.; Strano, M. S. Carbon Nanotubes: A Bright Future for Defects. *Nat. Chem.* **2013**, *5*, 812−813.

(18) Lyu, M.; Meany, B.; Yang, J.; Li, Y.; Zheng, M. Toward Complete Resolution of DNA/Carbon Nanotube Hybrids by Aqueous Two-Phase Systems. *J. Am. Chem. Soc.* **2019**, *141*, 20177−20186.

(19) Fagan, J. A.; Hároz, E. H.; Ihly, R.; Gui, H.; Blackburn, J. L.; Simpson, J. R.; Lam, S.; Hight Walker, A. R.; Doorn, S. K.; Zheng, M. Isolation of> 1 nm Diameter Single-Wall Carbon Nanotube Species Using Aqueous Two-Phase Extraction. *ACS Nano* **2015**, *9*, 5377−5390.

(20) Gui, H.; Chen, H.; Khripin, C. Y.; Liu, B.; Fagan, J. A.; Zhou, C.; Zheng, M. A Facile and Low-Cost Length Sorting of Single-Wall Carbon Nanotubes by Precipitation and Applications for Thin-Film Transistors. *Nanoscale* **2016**, *8*, 3467−3473.

(21) Wepasnick, K. A.; Smith, B. A.; Bitter, J. L.; Fairbrother, D. H. Chemical and Structural Characterization of Carbon Nanotube Surfaces. *Anal. Bioanal. Chem.* **2010**, *396*, 1003−1014.
(22) Mann, F. A.; Herrmann, N.; Meyer, D.; Kruss, S. Tuning Selectivity of Fluorescent Carbon Nanotube-Based Neurotransmitter Sensors. *Sensors* **2017**, *17*, 1521.
(23) Freeley, M.; Worthy, H. L.; Ahmed, R.; Bowen, B.; Watkins, D.; Macdonald, J. E.; Zheng, M.; Jones, D. D.; Palma, M. Site-Specific One-to-One Click Coupling of Single Proteins to Individual Carbon Nanotubes: A Single-Molecule Approach. *J. Am. Chem. Soc.* **2017**, *139*, 17834−17840.
(24) Freeley, M.; Attanzio, A.; Cecconello, A.; Amoroso, G.; Clement, P.; Fernandez, G.; Gesuele, F.; Palma, M. Tuning the Coupling in Single-Molecule Heterostructures: DNA-Programmed and Reconfigurable Carbon Nanotube-Based Nanohybrids. *Adv. Sci.* **2018**, *5*, 1800596.
(25) Danné, N.; Godin, A. G.; Gao, Z.; Varela, J. A.; Groc, L.; Lounis, B.; Cognet, L. Comparative Analysis of Photoluminescence and Upconversion Emission from Individual Carbon Nanotubes for Bioimaging Applications. *ACS Photonics* **2018**, *5*, 359−364.
(26) Larsen, B. A.; Deria, P.; Holt, J. M.; Stanton, I. N.; Heben, M. J.; Therien, M. J.; Blackburn, J. L. Effect of Solvent Polarity and Electrophilicity on Quantum Yields and Solvatochromic Shifts of Single-Walled Carbon Nanotube Photoluminescence. *J. Am. Chem. Soc.* **2012**, *134*, 12485−12491.
(27) Gao, J.; Gomulya, W.; Loi, M. A. Effect of Medium Dielectric Constant on the Physical Properties of Single-Walled Carbon Nanotubes. *Chem. Phys.* **2013**, *413*, 35−38.
(28) Roxbury, D.; Jena, P. V.; Shamay, Y.; Horoszko, C. P.; Heller, D. A. Cell Membrane Proteins Modulate the Carbon Nanotube Optical Bandgap via Surface Charge Accumulation. *ACS Nano* **2016**, *10*, 499−506.
(29) Zheng, Y.; Alizadehmojarad, A. A.; Bachilo, S. M.; Kolomeisky, A. B.; Weisman, R. B. Dye Quenching of Carbon Nanotube Fluorescence Reveals Structure-Selective Coating Coverage. *ACS Nano* **2020**, *14*, 12148−12158.
(30) Salem, D. P.; Gong, X.; Liu, A. T.; Koman, V. B.; Dong, J.; Strano, M. S. Ionic Strength-Mediated Phase Transitions of Surface-Adsorbed DNA on Single-Walled Carbon Nanotubes. *J. Am. Chem. Soc.* **2017**, *139*, 16791−16802.
(31) Hou, Z.; Tumiel, T. M.; Krauss, T. D. Spatially Resolved Photoluminescence Brightening in Individual Single-Walled Carbon Nanotubes. *J. Appl. Phys.* **2021**, *129*, No. 014305.
(32) Qu, H.; Rayabharam, A.; Wu, X.; Wang, P.; Li, Y.; Fagan, J.; Aluru, N. R.; Wang, Y. Selective filling of n-hexane in a tight nanopore. *Nat. Commun.* **2021**, *12*, 310.
(33) Jena, P. V.; Safaee, M. M.; Heller, D. A.; Roxbury, D. DNA-Carbon Nanotube Complexation Affinity and Photoluminescence Modulation Are Independent. *ACS Appl. Mater. Interfaces* **2017**, *9*, 21397−21405.
(34) Utech, S.; Boccaccini, A. R. A Review of Hydrogel-Based Composites for Biomedical Applications: Enhancement of Hydrogel Properties by Addition of Rigid Inorganic Fillers. *J. Mater. Sci.* **2016**, *51*, 271−310.
(35) Wang, B.; Wan, Y.; Zheng, Y.; Lee, X.; Liu, T.; Yu, Z.; Huang, J.; Ok, Y. S.; Chen, J.; Gao, B. Alginate-Based Composites for Environmental Applications: A Critical Review. *Crit. Rev. Environ. Sci. Technol.* **2019**, *49*, 318−356.
(36) Sun, X.; Agate, S.; Salem, K. S.; Lucia, L.; Pal, L. Hydrogel-Based Sensor Networks: Compositions, Properties, and Applications—A Review. *ACS Appl. Bio Mater.* **2021**, *4*, 140−162.
(37) Duque, J. G.; Pasquali, M.; Cognet, L.; Lounis, B. Environmental and Synthesis-Dependent Luminescence Properties of Individual Single-Walled Carbon Nanotubes. *ACS Nano* **2009**, *3*, 2153−2156.
(38) Nash, M. E.; Carroll, W. M.; Foley, P. J.; Maguire, G.; O'Connell, C.; Gorelov, A. V.; Beloshapkin, S.; Rochev, Y. A. Ultra-Thin Spin Coated Crosslinkable Hydrogels for Use in Cell Sheet Recovery—Synthesis, Characterisation to Application. *Soft Matter* **2012**, *8*, 3889−3899.
(39) Simpliciano, C.; Clark, L.; Asi, B.; Chu, N.; Mercado, M.; Diaz, S.; Goedert, M.; Mobed-Miremadi, M., *Cross-Linked Alginate Film Pore Size Determination Using Atomic Force Microscopy and Validation Using Diffusivity Determinations*; Scientific Research Publishing Inc.: 2013.
(40) Tummala, N. R.; Striolo, A. SDS Surfactants on Carbon Nanotubes: Aggregate Morphology. *ACS Nano* **2009**, *3*, 595−602.
(41) Lee, B.-H.; Li, B.; Guelcher, S. A. Gel Microstructure Regulates Proliferation and Differentiation of MC3T3-E1 Cells Encapsulated in Alginate Beads. *Acta Biomater.* **2012**, *8*, 1693−1702.
(42) Roxbury, D.; Jena, P. V.; Williams, R. M.; Enyedi, B.; Niethammer, P.; Marcet, S.; Verhaegen, M.; Blais-Ouellette, S.; Heller, D. A. Hyperspectral Microscopy of Near-Infrared Fluorescence Enables 17-Chirality Carbon Nanotube Imaging. *Sci. Rep.* **2015**, *5*, 14167.
(43) Shankar, A.; Mittal, J.; Jagota, A. Binding Between DNA and Carbon Nanotubes Strongly Depends Upon Sequence and Chirality. *Langmuir* **2014**, *30*, 3176−3183.
(44) Hu, X.; Ji, J. Covalent Layer-by-Layer Assembly of Hyperbranched Polyether and Polyethyleneimine: Multilayer Films Providing Possibilities for Surface Functionalization and Local Drug Delivery. *Biomacromolecules* **2011**, *12*, 4264−4271.
(45) Gillen, A. J.; Kupis-Rozmysłowicz, J.; Gigli, C.; Schuergers, N.; Boghossian, A. A. Xeno Nucleic Acid Nanosensors for Enhanced Stability Against Ion-Induced Perturbations. *J. Phys. Chem. Lett.* **2018**, *9*, 4336−4343.
(46) Jin, H.; Jeng, E. S.; Heller, D. A.; Jena, P. V.; Kirmse, R.; Langowski, J.; Strano, M. S. Divalent Ion and Thermally Induced DNA Conformational Polymorphism on Single-walled Carbon Nanotubes. *Macromolecules* **2007**, *40*, 6731−6739.
(47) Wei, L.; Li, L.-J.; Chan-Park, M. B.; Yang, Y.; Chen, Y. Aggregation-Dependent Photoluminescence Sidebands in Single-Walled Carbon Nanotube. *J. Phys. Chem. C* **2010**, *114*, 6704−6711.
(48) Huang, B.; Bates, M.; Zhuang, X. Super-Resolution Fluorescence Microscopy. *Annu. Rev. Biochem.* **2009**, *78*, 993−1016.

https://doi.org/10.1021/acsami.1c06562
ACS Appl. Mater. Interfaces XXXX, XXX, XXX−XXX